RSC Advances

PAPER

View Article Online
View Journal | View Issue

Cite this: *RSC Adv.*, 2015, **5**, 67054

Novel halogen-free flame retardants based on adamantane for polycarbonate

Shu-Qin Fu, Jian-Wei Guo,* Dong-Yu Zhu, Zhe Yang, Chu-Fen Yang, Jia-Xing Xian and Xiong Li

A novel series of flame retardants (FRs) containing phosphate moieties attached to a bridgehead-substituted adamantane, 1-(diphenyl phosphate) adamantane (DPAd), 1,3-bis(diphenyl phosphate) adamantane (BDPAd), 1,3,5-tris(diphenyl phosphate) adamantane (TDPAd) and 1,3,5,7-tetrakis(diphenyl phosphate) adamantane (TKDPAd), were systematically synthesized in an attempt to develop efficient FRs for polycarbonate (PC). Their chemical structures were confirmed by Fourier Transform Infrared Spectroscopy (FTIR), Nuclear Magnetic Resonance (^{1}H and ^{31}P NMR), elemental analysis and melting point measurements. The flame-retarding efficiencies of the FRs were evaluated by Limited Oxygen Index (LOI), UL-94 vertical burning experiments, Scanning Electron Microscopy (SEM), Cone Calorimeter Test (CCT), Thermogravimetric Analysis (TGA), FTIR and TGA-FTIR. For TKDPAd, thermal decomposition took place in a sharply two-step mechanism at high temperature above 381.5 °C. A significant improvement of flame-retardant performance in PC/TKDPAd among the PC/FR was observed with an addition of 8 wt% TKDPAd in the presence of an anti-dripping agent (0.1 wt%). High thermal stability and phosphorus content of flame retardant are believed to be of great importance for efficient flame-retardant action of adamantane-based phosphates.

Received 8th June 2015
Accepted 28th July 2015

DOI: 10.1039/c5ra10887j

www.rsc.org/advances

1. Introduction

Traditional materials such as metals and woods are now gradually being replaced by polymers. However, polymers are easily flammable and subjected to various mandatory controls for safety reasons.[1–3] The thermal stability of polycarbonate (PC) meets the requirements for application in advanced electronics and construction materials.[4] Due to its relatively high tendency of char formation, PC gives a limiting oxygen index (LOI) value of typically 26% and a UL-94 V-2 rating. However, for safety concerns, more stringent flame retardant performances of PC composites are often required.[5,6] To decrease the combustibility of the polymers, researchers have made great efforts to the development of the flame retardants (FRs).[7–11] As part of the development of halogen-free FRs to replace bromo-aromatic FRs, the development of phosphorus-containing compounds generating less toxic gases and smoke gradually become the main focus.[12–15]

Among the various phosphorus compounds, aryl phosphates like triphenyl phosphate (TPP) and resorcinol bis(diphenyl phosphate) (RDP) are the most widely used FRs and exhibit fairly good fire-retarding performances for polyesters and their blends.[6,16,17] Jang *et al.* reported that PC was not only stabilized but delayed the degradation process by TPP or RDP; and part amounts of TPP or RDP occurred an alcoholysis reaction with the alcohol products from the decomposed PC, which are related during the latter part of thermal degradation.[18] Nonetheless, considerable amounts of TPP and RDP that evaporate in the beginning mass loss region decrease their ability of stabilizing the carbonate linkage of PC. The decomposition temperature of the flame retardant is a major parameter controlling the flame retardancy mode of action. It shows that matching the decomposition temperature of PC promotes char formation from PC in the pyrolysis zone.[19,20] Marie-Claire Despinasse *et al.* found that using an aryl phosphate mixture of BDP and HDP to match the decomposition temperature of PC is possible to enhance the charring of PC in the condensed phase.[21] The temperature matching is also likely by varying the structure of the bridging unit or the end group of the aryl phosphate oligomers. However, the bridging unit can vary in chemical structure, such as can be rigid or flexible, aromatic or aliphatic, hydrophobic or hydrophilic. Congtranh Nguyen *et al.* also showed that the decomposition temperature and char residue of ethylene glycol bis(diphenyl phosphate) (ethylene glycol as bridging unit) were lower than RDP (resorcinol as bridging unit), which revealed the relationships of the effect of the chemical structure of bridging unit on thermal stability and flame-retarding ability.[22] The substitution of the phenyl end group also strongly influences the reactivity of the flame retardant.[23] Further, phosphorus content is believed to be the most vital factor on flame retardancy in recent years.[24–26] However, the

School of Chemical Engineering & Light Industry, Guangdong University of Technology, Guangzhou 510006, P. R. China. E-mail: guojw@gdut.edu.cn

relationships of fire-retarding efficiencies and thermal degradation behaviors among bridging unit, phosphorus content and substitution amounts of the bridging unit were not clearly revealed so far.

In this paper, incorporation of adamantane group into the molecular structures of FRs was performed by reacting aryl phosphates with adamantane compounds to further improve the thermal stability of conventional FRs. The particular structure of adamantane imparts its derivatives with many useful chemical and physical properties, such as bulky and tetrahedral geometry, extreme lipophilicity, good thermal and oxidative stabilities, and innocuity, *etc.*[27–31] Pyrolysis has been carried out using TGA in air to simulate the real combustion. The relationships among bridging unit (adamantane), phosphorus content and substitution amounts of adamantane on thermal stability, fire performances and degradation behaviors of PC were investigated through TGA, TGA-FTIR, LOI, UL-94 vertical burning, CCT, SEM. The solid residues after pyrolysis were analyzed by FTIR.

2. Experimental

2.1 Materials

Polycarbonate 301-10 was provided by Dow Chemical Company (America) and was dried at 120 °C for 8 h before use. Adamantane (CP), 1-hydroxyadamantane and 1,3-dihydroxyadamantane were purchased from Hangzhou Yang Li petrochemical co., LTD (Hangzhou, China). Diphenyl phosphoryl chloride (AR) was obtained from Aladdin Industrial Corporation (Shanghai, China). Pyridine was distilled by anhydrous calcium chloride before use. All reagents commercially available were used as received unless otherwise stated. 1,3,5-Trihydroxyadamantane and 1,3,5,7-tetrahydroxyadamantane were prepared according to the published procedures.[32,33]

2.2 Synthesis

A series of adamantane-based phosphates are successfully synthesized and their structures are given in Table 1. The general synthetic routes are shown in Scheme 1.

2.2.1 Synthesis of 1-(diphenyl phosphate) adamantane (DPAd). Diphenyl phosphoryl chloride (9.50 g, 30.00 mmol) was added in small portions over 30 min to an intensively stirred mixture of 1-hydroxyadamantane (4.50 g, 29.00 mmol) and pyridine (11.70 g, 150.00 mmol) at 60 °C. The mixture was then slowly heated to 95 °C and held at that temperature for 3 h. The solvent was evaporated at reduced pressure once the reaction mixture was cooled to room temperature, and then the oil resultant was dissolved in 100 ml of ethyl acetate. The solution was washed successively with water 2 × 100 ml, HCl (1 M, 2 × 100 ml), aq. Na_2CO_3 (15 wt%, 2 × 100 ml), and distilled water 2 × 100 ml, dried over Na_2SO_4 and evaporated to dryness and heated for 12 h under vacuum at 45 °C. The crude product was purified by recrystallizing with ethyl acetate/*n*-hexane to give product DPAd (9.90 g, 88.2% yield) as white solid powder. ^{1}H NMR (400 MHz, DMSO-d_6) δ: 7.39–7.21 (t, 10H, C_6H_5), 2.15–2.05 (d, 9H, H_{ad}-2,3,5,7,8,10, this "ad" means adamantane), 1.58 ppm (s, 6H, H_{ad}-4,6,9); FT-IR (KBr) ν: 2912, 2855, 1591, 1489, 1284, 1196, 1010, 941, 764 cm^{-1}. Anal. calcd for $C_{22}H_{25}O_4P$: C, 68.74, H, 6.56; found: C, 68.79, H, 6.62.

2.2.2 Synthesis of 1,3-bis(diphenyl phosphate) adamantane (BDPAd). Synthesis of BDPAd was similar to that in 2.2.1, except 1,3-dihydroxyadamantane (4.00 g, 23.80 mmol) was used to instead of 1-hydroxyadamantane, giving white solid BDPAd (12.50 g, 83.0% yield). ^{1}H NMR (400 MHz, DMSO-d_6) δ: 7.38–7.20 (t, 20H, C_6H_5), 2.38–2.35 (m, 4H, H_{ad}-2,5,7), 2.00 (s, 8H, H_{ad}-4,8,9,10), 1.47 ppm (s, 2H, H_{ad}-6); FT-IR (KBr) ν: 2926, 2867, 1589, 1492, 1300, 1281, 1195, 984, 957, 932, 782 cm^{-1}. Anal. calcd for $C_{34}H_{34}O_8P_2$: C, 64.56, H, 5.42; found: C, 64.57, H, 5.47.

2.2.3 Synthesis of 1,3,5-tris(diphenyl phosphate) adamantane (TDPAd). A solution of chromium trioxide (100.00 g, 1000.00 mmol) in distilled water (100 ml) was added dropwise to the solution of adamantane (13.60 g, 100 mmol) in glacial acetic acid (100 ml) with continuous stirring at 95–98 °C. After the completion of dropping, the mixture was stirred for an additional 1 h at 100 °C. The solution was evaporated and the residue was neutralized by 40 wt% aq. KOH. The mixture was extracted with ethyl acetate (500 ml) at 70 °C for five times to give white crystal 1,3,5-trihydroxyadamantane (8.50 g, 50.0% yield). ^{1}H NMR (400 MHz, DMSO-d_6) δ: 4.49 (s, 3H, O*H*), 2.11 (s, 1H, H_{ad}-7), 1.33–1.42 ppm (m, 12H, H_{ad}-2,4,6,8,9,10); anal. calcd for $C_{10}H_{16}O_3$: C, 65.19, H, 8.17; found: C, 65.19; H, 8.23.

Diphenyl phosphoryl chloride (10.30 g, 38.20 mmol) was added in small portions over 30 min to a vigorously stirring mixture of 1,3,5-trihydroxyadamantane (2.00 g, 10.90 mmol) and pyridine (15.00 g, 189.00 mmol) at 70 °C. The mixture was then slowly heated to 90 °C and held at that temperature for 7 h. The solvent was evaporated at reduced pressure once the reaction mixture was cooled to room temperature, and then the oil resultant was dissolved in 100 ml of CH_2Cl_2. The solution was washed successively with water 3 × 100 ml, HCl (1 M, 3 × 100 ml), aq. Na_2CO_3 (15 wt%, 3 × 100 ml), and distilled water 3 × 100 ml, dried over Mg_2SO_4, evaporated to dryness and heated for 12 h under vacuum at 50 °C. The crude product was purified by silica gel chromatography eluted with ethyl acetate : *n*-hexane = 1 : 10 to give product TDPAd (6.00 g, 62.5% yield) as greenish paste. ^{1}H NMR (400 MHz, $CDCl_3$) δ: 7.55–7.16 (m, 30H, C_6H_5), 2.52 (d, 6H, H_{ad}-2,4,9), 2.05–1.96 ppm (t, 7H, H_{ad}-6,7,8,10). FT-IR (KBr) ν: 2956, 2873, 1590, 1489, 1292, 1220, 1190, 1100, 1015, 952, 772 cm^{-1}. Anal. calcd for $C_{46}H_{43}O_{12}P_3$: C, 62.73, H, 4.92; found: C, 62.71, H, 4.97.

2.2.4 Synthesis of 1,3,5,7-tetrakis(diphenyl phosphate) adamantane (TKDPAd). 1,3,5,7-Tetrabromoadamantane and 1,3,5,7-tetrahydroxyadamantane were prepared by modifying published procedures.[33]

Adamantane (4.86 g, 35.75 mmol) was added in small portions over 30 min to a stirring mixture of bromine (22.50 ml) and anhydrous aluminum chloride (5.00 g, 37.50 mmol) at 0–3 °C. The mixture was then slowly heated to 70 °C and held at that temperature for 24 h. Hydrogen bromide evolved vigorously during the addition and heating. The reaction mixture was treated subsequently with aqueous sodium sulfite and hydrochloric acid. The resulting solid was filtered, dried in vacuum,

Table 1 Fundamental parameters of the FRs employed in this study

Abbreviation	Full name	Molecular formula	Structural formula	P content[a] (%)	MP[a] (°C)
DPAd	1-(Diphenyl phosphate) adamantane	$C_{22}H_{25}O_4P$	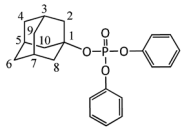	8.06	53.3
BDPAd	1,3-Bis(diphenyl phosphate) adamantane	$C_{34}H_{34}O_8P_2$	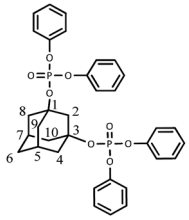	9.79	100.4
TDPAd	1,3,5-Tris(diphenyl phosphate) adamantane	$C_{46}H_{43}O_{12}P_3$	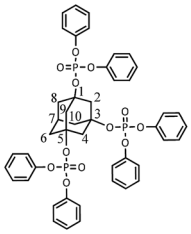	10.56	Liquid
TKDPAd	1,3,5,7-Tetrakis(diphenyl phosphate) adamantane	$C_{58}H_{52}O_{16}P_4$	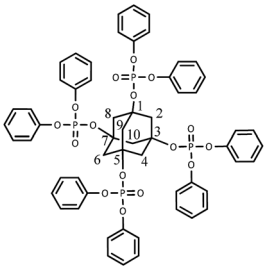	10.97	77.5

[a] P content = phosphorous content; MP = melting pointing.

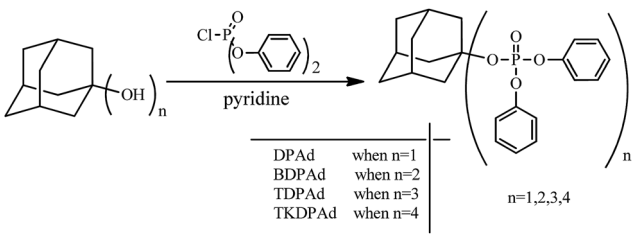

Scheme 1 Synthetic routes for the FRs employed in this study.

and recrystallized from CH_3CN to give tan crystals (10.10 g, 63.0% yield); mp: 246–248 °C; ^{1}H NMR (400 MHz, $CDCl_3$) δ: 2.71 ppm (s, 12H); anal. calcd for $C_{10}H_{12}Br_4$: C, 26.58; H, 2.68. Found: C, 26.66; H, 2.68.

1,3,5,7-Tetrabromoadamantane (8.34 g, 18.44 mmol) and Ag_2SO_4 (12.76 g, 40.90 mmol) were suspended in concentrated sulfuric acid (20 ml) and the mixture was slowly heated to 80 °C and stirred at that temperature for 7 h. After cooling, the AgBr precipitate was removed by filtration and the solution was rinsed with water. The filtrate was neutralized with KOH and evaporated. The resulting gray residue was dried and then extracted 24 h with ethanol in a Soxhlet apparatus. After evaporation of the ethanol, the residue was dissolved in methanol and filtered. Recrystallization from MeOH/acetone yielded a white solid (2.88 g, 78.0% yield); MP: 316–318 °C; ^{1}H NMR (400 MHz, DMSO-d_6) δ: 4.58 (s, 4H), 1.36 ppm (s, 12H); anal. calcd for $C_{10}H_{16}O_4$: C, 59.98; H, 8.05. Found: C, 59.92; H, 8.11.

Diphenyl phosphoryl chloride (12.80 g, 48.00 mmol) was added in small portions over 30 min to an intensively stirring mixture of 1,3,5,7-tetrahydroxyadamantane (2.00 g, 10.00 mmol) and pyridine (18.57 g, 235.00 mmol) at 70 °C. The mixture was then slowly heated to 90 °C and held at that temperature for 9 h. The solvent was evaporated at reduced pressure once the reaction mixture was cooled to room temperature, and then the resultant was dissolved in 100 ml of CH_2Cl_2. The solution was washed successively with water 3 × 100 ml, HCl (1 M, 3 × 100 ml), aq. Na_2CO_3 (15 wt%, 3 × 100 ml), and distilled water 3 × 100 ml, dried over Na_2SO_4 and evaporated to dryness and heated for 8 h under vacuum at 50 °C. The

crude product was purified by silica gel chromatography eluted with petroleum ether : diethyl ether = 1 : 4 to give product TKDPAd (6.52 g, 61.8% yield) as white crystal. ^{1}H NMR (400 MHz, $CDCl_3$) δ: 7.29–7.16 (dt, 40H, C_6H_5), 2.54 ppm (s, 12H, H_{ad}-2,4,6,8,9,10); FTIR (KBr) ν: 3059, 1590, 1488, 1291, 1190, 1020, 958, 942, 772 cm^{-1}. Anal. calcd for $C_{58}H_{52}O_{16}P_4$: C, 61.71; H, 4.64. Found: C, 61.72; H, 4.60.

2.2.5 Preparation of PC/DPAd, PC/BDPAd, PC/TDPAd and PC/TKDPAd composites. PC, FRs and anti-dripping agent were dried in a vacuum oven at 110 °C and 50 °C for 6 h before used, respectively. Then PC, FR and anti-dripping agent (0.1 wt%) were melt-mixed in an internal mixer (KY-3220-2L, Dongguan Houjie Machinery Equipment factory, China) at 250 °C for 10 min. The prepared composites were molded under compression (15 MPa) at 250 °C for 10 min and cooled to room temperature naturally to obtain PC/FR compositions sheets with standard size for further testing. The formulations of the PC/FR compositions are listed in Table 2.

2.3 Measurements and sample preparation

2.3.1 Spectroscopic analysis. ^{1}H and ^{31}P spectra of synthesized intermediates and the final product were obtained by using a Bruker AVANCE III 400 MHz superconducting Fourier in dimethyl sulfoxide-d_6 (DMSO-d_6) or deuteron-chloroform ($CDCl_3$) solution and were referenced to external tetramethylsilane (TMS). FTIR spectra were obtained by using a Thermo Electron Nicolet-6700 FTIR spectrometer with a scanning number of 16. A finely ground, approximately 1% mixture of a solid sample in KBr powders is fused into a transparent disk for FTIR measurement using a hydraulic press. The elemental analysis was performed with a Perkin Elmer Series II 2400 elemental analyzer.

2.3.2 Limiting oxygen index (LOI) test. The LOI test was performed by using a DM-4022 oxygen index apparatus with a magneto-dynamic oxygen analyzer, according to ASTM D2863-97 standard. The average values of LOI were obtained from the results of six tests.

2.3.3 UL-94 vertical burning test. The UL-94 vertical burning test was carried out based on AG5100A vertical-horizontal burning apparatus according to ASTM D3801 standard. The average values of UL-94 were obtained from the results of five tests.

2.3.4 Scanning electron microscopy (SEM). The SEM observation was performed on a Hitachi S-3400N scanning electron microscope to investigate the morphologies of the residual chars. The char samples for SEM were obtained after combustion in the LOI test and were made electrically conductive by sputter coating with a thin layer of gold–palladium alloy. The images were taken in high vacuum mode with 15 kV acceleration voltage and a medium spot size.

2.3.5 Cone calorimeter test (CCT). The CCT was carried out by using a cone calorimeter (Fire Testing Technology, UK) according to ISO5660 standard procedures. Each specimen, with a dimension of 100 mm × 100 mm × 3 mm, was wrapped in an aluminum foil and exposed horizontally to an external heat flux of 35 kW m^{-2}. All the samples were run in duplicate, and the average value was recorded.

2.3.6 Thermal analysis. The TGA experiments were performed under an air atmosphere using a NETZSCH STA 409 PC thermal gravimetric analyzer. The samples with a mass of about 8 mg were placed in an aluminum crucible and ramped from room temperature up to about 800 °C at a heating rate of 10 °C min^{-1}, while the flow of air was maintained at 50 ml min^{-1}.

The TGA-FTIR experiments were carried out by using a 409 PC thermal analyzer (Netzsch, Germany) coupled with a Nicolet-6700 FTIR (Thermofisher, USA). About 8 mg of each sample was heated from room temperature to 800 °C at a heating rate of 10 °C min^{-1} under nitrogen (flow rate = 50 ml min^{-1}). The couple system between TGA and FTIR was a quartz capillary kept at temperature of 220 °C. The spectra were acquired in the range of 4000 cm^{-1} to 650 cm^{-1}.

Table 2 LOI, UL-94 results for PC and PC/FR composites

				UL-94	
FR	P content (%)	PC/FR (wt/wt)	LOI (%)	Ranking	Dripping
DPAd	8.06	100/0	26.1	V-2	Yes
		94/6	27.1	V-2	Yes
		92/8	27.3	V-2	Yes
		90/10	27.3	V-2	Yes
		88/12	27.6	V-2	Yes
BDPAd	9.79	94/6	27.6	V-2	Yes
		92/8	27.6	V-2	Yes
		90/10	28.2	V-1	No
		88/12	29.1	V-1	No
TDPAd	10.56	94/6	27.6	V-1	No
		92/8	28.3	V-0	No
		90/10	29.1	V-0	No
		88/12	30.0	V-0	No
TKDPAd	10.97	94/6	28.6	V-1	No
		92/8	29.1	V-0	No
		90/10	30.1	V-0	No
		88/12	32.0	V-0	No

3. Results and discussion

3.1 Synthesis of the FRs

Synthesis of the FRs based on rigid adamantane ring structure, were performed in good yields according to Scheme 1. For the similar structures of the FRs, which were measured by FTIR, ^{1}H and ^{31}P NMR displayed in Fig. 1, 2 and 3, respectively, TKDPAd was taken as the only example to analyze its structure here.

FTIR spectrum of phosphorus-containing TKDPAd shown in Fig. 1D exhibited the characteristic CH_2 group absorption at 3059 cm^{-1}. The 1590 cm^{-1} and 1488 cm^{-1} to the vibration with C=C. Stretches at 1291 and 1190 cm^{-1} are attributed to the absorptions of resonances of P=O and P–O–C (aromatic), respectively, which are characteristic of phosphorus compounds. The 772 cm^{-1} stretch is caused by the attachment of phosphonate group on the adamantane ring. The strong absorptions at 1020 cm^{-1}, 958 cm^{-1}, 942 cm^{-1} are ascribed to P–O stretching.

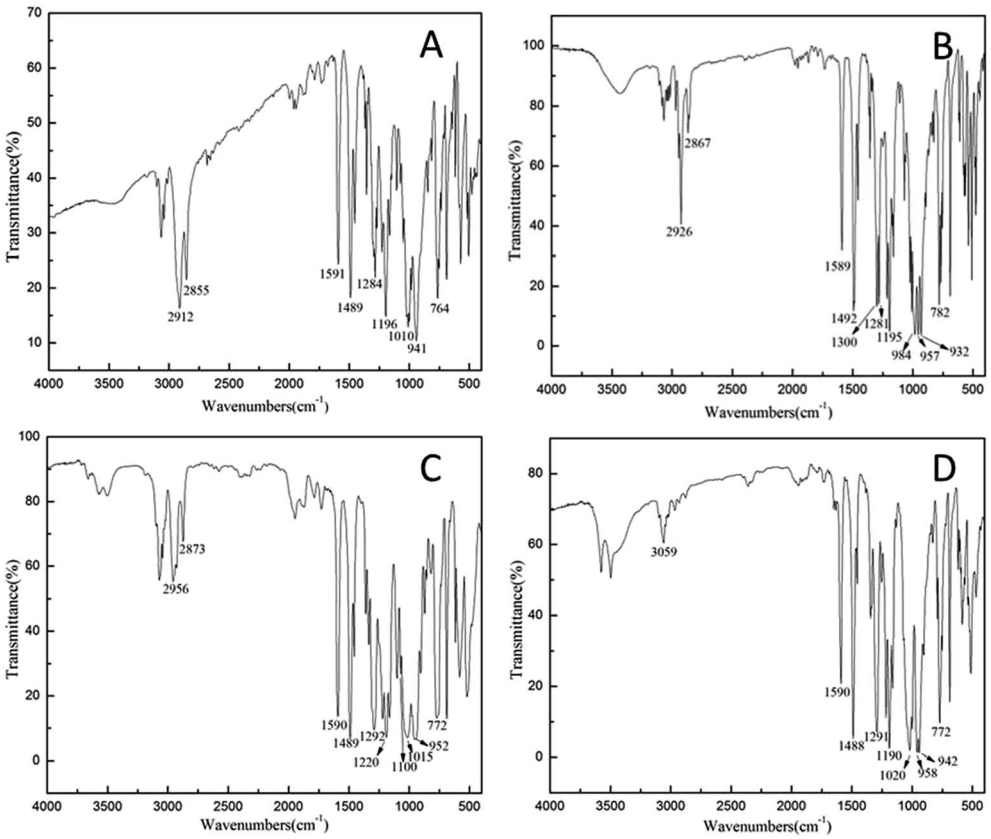

Fig. 1 FTIR spectra of the FRs employed in this study: (A) DPAd, (B) BDPAd, (C) TDPAd, and (D) TKDPAd.

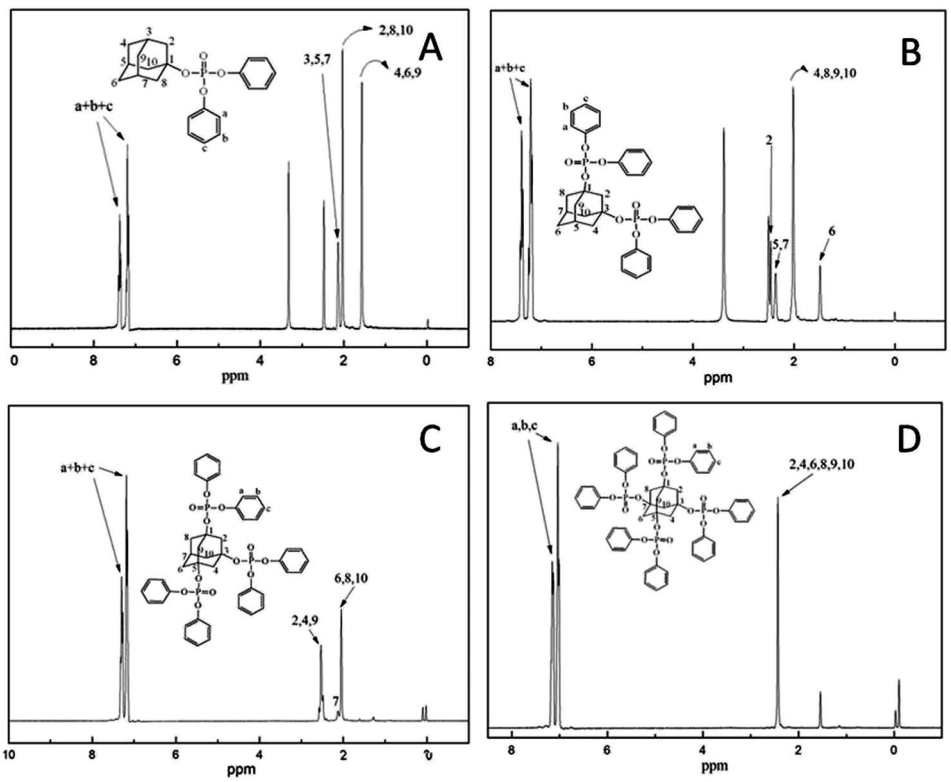

Fig. 2 ^{1}H NMR spectra of the FRs employed in this study: (A) DPAd, (B) BDPAd, (C) TDPAd, and (D) TKDPAd.

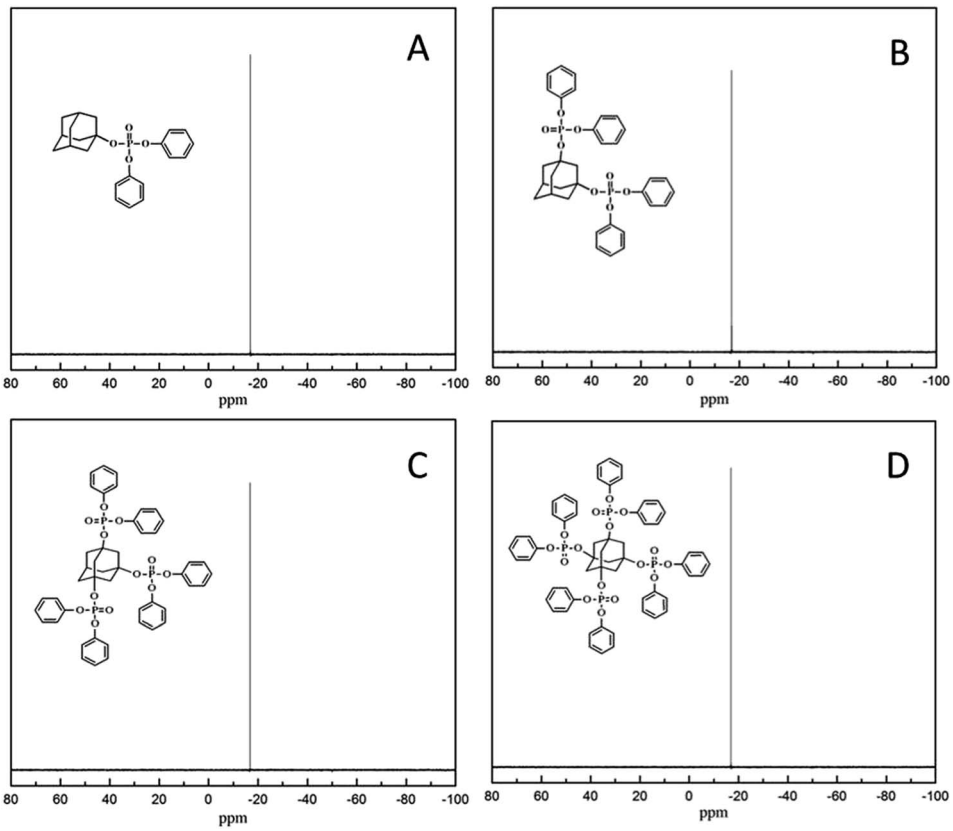

Fig. 3 ^{31}P NMR spectra of the FRs employed in this study: (A) DPAd, (B) BDPAd, (C) TDPAd, and (D) TKDPAd.

^{1}H and ^{31}P NMR shown in Fig. 2D and 3D, respectively, were employed to further confirm its chemical structure. The chemical shifts at 7.29–7.16 ppm are attributed to the aromatic protons labeled (a–c). A strong resonance signal at 2.54 ppm is characteristic of the protons (labeled 2, 4, 6, 8, 9, 10) of CH_2 groups in adamantyl. The single peak observed at −16.99 ppm in ^{31}P NMR spectrum suggesting the unique phosphorus compound. These NMR data are self-consistent with the results of FTIR described above, confirming the successful synthesis of high-purity TKDPAd.

3.2 Flammability characteristics

3.2.1 Limiting oxygen index (LOI) and UL-94 vertical burning test. The flammability characteristics of PC blended with FRs added in amounts of 6–12 wt% in the presence of an anti-dripping agent (0.1 wt%) were first evaluated by the LOI and UL-94 vertical measurements, respectively, and the corresponding results were summarized in Table 2.

From the Table 2, the LOI values increase with the addition content of FRs. The LOI value of PC here is 26.1% and those of composites containing 6–12 wt% FRs are 27.1–32.0%. The LOI values of PC composites can be slightly enhanced with DPAd from 26.1% (PC) to 27.3% (PC/12 wt% DPAd). However, it is expected to notice that the PC/TKDPAd exhibits high values of LOI over 28.6%, significantly greater than that of the neat PC. The conclusion about relative flame-retarding efficiency of FR can be withdrawn from the results is that, the increase of P content and the substitution amounts of adamantane in the FRs is effective for the enhancement of LOI of PC/FR significantly.

The UL-94 vertical burning experiment is considered as another important means for determining the upward burning characteristics of PC/FR. The results of UL-94 vertical burning test of these PC/FR compositions are summarized in Table 2. As was expected, PC/FR achieved the V-0 classification in UL-94 test by loading different amounts of the FRs except DPAd, respectively. Especially, addition of 8 wt% TKDPAd provided V-0 rating and no dropping for PC/FR, which showed that the P content was actually a vital factor on flame retardancy of the adamantane-based phosphates. At the end of burning experiments, the surfaces of these PC/FR compositions were covered with an expanded char structure, indicating that the PC/FR compositions formed an effective char which was able to prevent the heat transfer and flame spread during combustion.

3.2.2 Cone calorimeter test (CCT). Flame-retarding efficiencies of the 8 wt% loading of FRs in PC were evaluated by a cone calorimeter. CCT is becoming one of the most effective methods for assessing the fire behaviors of materials and brings quantitative analysis to the flame retardancy of materials by investigating some parameters, such as heat release rate (HRR), peak of HRR (pHRR) and the total heat release (THR).[34] The HRR curves and THR curves of PC and PC/FR compositions are showed in Fig. 4A and B, respectively.

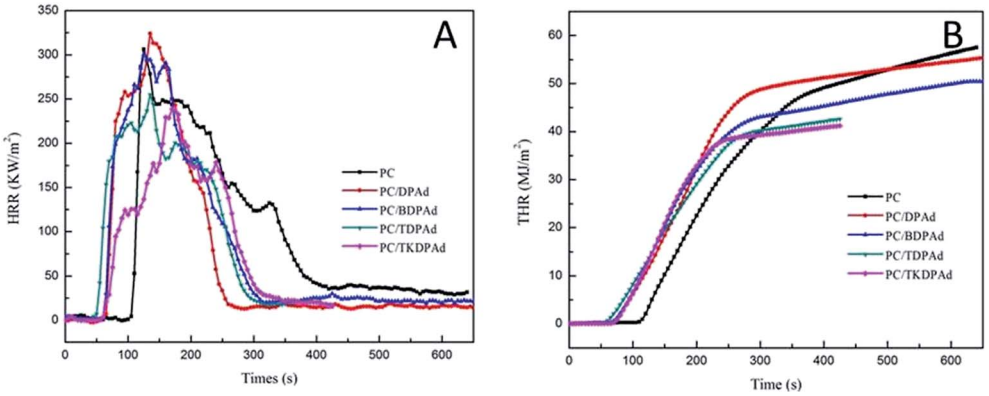

Fig. 4 HRR (A) and THR (B) curves of PC and PC/FR composites.

The HRR, particularly the pHRR, has been believed to be one of the most important parameters to evaluate the fire safety of material.[35] As can be seen in Fig. 4A, with the increasing emission of flammable gases into the air, the neat PC burned fiercely at about 110 s of ignition to reach the pHRR of (306 ± 30) kW m^{-2} and exhibited a sharp peak with some small shoulders after. Under the radiation of a 35 kW m^{-2} heat flux, the surface of the neat PC melted to form an integral but thin char layer first, which corresponded to the appearance of the small shoulders of the HRR curve of PC in Fig. 4A. Then the surface of the formed char layer was damaged by the emission of vigorous gases from the underlying compositions and the porous char structure was formed gradually.[36] After about 400 s as seen in Fig. 4A, most of the PC/FR compositions have been burnt out and the HRR always keeps above zero till the test stopped, which is due to the slow degradation of the leaving char residue.

However, Fig. 4A shows that there is a mainly small shoulder before reaching the pHRR of PC/FR, which means the FRs employed in this study could facilitate PC decomposition in the earlier stage. In other words, the FRs could promote char formation of PC compositions during combustion. From the HRR curves of PC/FR compositions in Fig. 4A, it presents a steady decrease of HRR value after an initial increase to form the char layer. An obvious peak (pHRR) of 324 ± 12 (PC/DPAd), 301 ± 14 (PC/BDPAd), 255 ± 12 (PC/TDPAd) and 240 ± 20 (PC/TKBDPAd) kW m^{-2} can be found in the HRR curves of the FRs. Although the pHRR of PC/DPAd compositions is slightly higher than that of the neat PC, the average of HRR (av-HRR) of the former is lower (90 ± 10 kW m^{-2}) than that of the latter (94 ± 10 kW m^{-2}), which means DPAd is still an efficient FR. It is easy to find that with the increase of P content and substitution amounts on adamantane, the pHRR and av-HRR (89 ± 8, 79 ± 7, 79 ± 7 kW m^{-2} for PC/BDPAd, PC/TDPAd, PC/TKDPAd, respectively) decreased significantly. And a terse residue layer covered on the aluminum foil could be observed. The decrease of pHRR and av-HRR can be attributed to the formation of compact and expansion of the residue layer stopped the spread of the heat and oxygen, and the emissions of volatile products.[37] The residue layer could keep the PC compositions thermal stability and improve its flame retardancy.

Moreover, the THR curves of PC and PC/FR compositions are shown in Fig. 4B. It is observed that the THR decreases from 61 ± 15 MJ m^{-2} (the neat PC) to 54 ± 11 MJ m^{-2} (PC/DPAd), 50 ± 10 MJ m^{-2} (PC/BDPAd), 43 ± 11 MJ m^{-2} (PC/TDPAd) and 41 ± 13 MJ m^{-2} (PC/TKDPAd), respectively, which indicates that part of the PC/FR compositions has not fully combusted, possibly undergoing a char-forming process, which can be attribute to the addition of the FRs. In other words, the adamantane-based phosphates could reduce the flammability and improve the flame retardant efficiency of PC compositions to be potential FRs. The flame-retarding efficiencies were improved significantly with the increase of P content and substitution amounts on adamantane. And it is believed the lower HRR and THR are relate to the condensed phase and mean the better flame retardation of FRs.[38]

3.3 Thermal degradation behaviors

3.3.1 TGA test. The thermal properties of the FRs and the 8 wt% loading of FRs in PC have been evaluated by TGA under air atmosphere as shown in Fig. 5 and Table 3. Fig. 5A shows the TGA curves (Fig. 5A1 for TG curves and Fig. 5A2 for DTG curves) for the FRs employed in this study from room temperature to 800 °C at a heating rate of 10 °C min^{-1} under air atmosphere.

There are two distinct thermal degradation behaviors to be noticeable in Fig. 5A. DPAd and BDPAd show a gently two-step degradation and little amounts of charred residues (6.4% for DPAd and 9.0% for BDPAd) at 800 °C while TKDPAd shows a sharply two-step degradations leaving higher charred residue (11.9%). However, TDPAd also shows a sharply two-step degradations, but leaving very little amounts of charred residue (4.5%) at 800 °C. Next to a sufficient flame-retarding effect, FRs for PC should meet two vital requirements: (a) good thermal stability for high processing temperatures (225–310 °C), and (b) sufficient compatibility with PC. Moreover, the difference in initial decomposition temperature ($T_{5\%}$) of the FRs became more pronounced as the phosphorus content was increased. However, Table 3 shows that DPAd already starts to decompose at 215.7 °C under an air atmosphere. In contrast to DPAd, the $T_{5\%}$ of decompositions for BDPAd, TDPAd and TKDPAd are shifted towards a higher temperature, indicating an

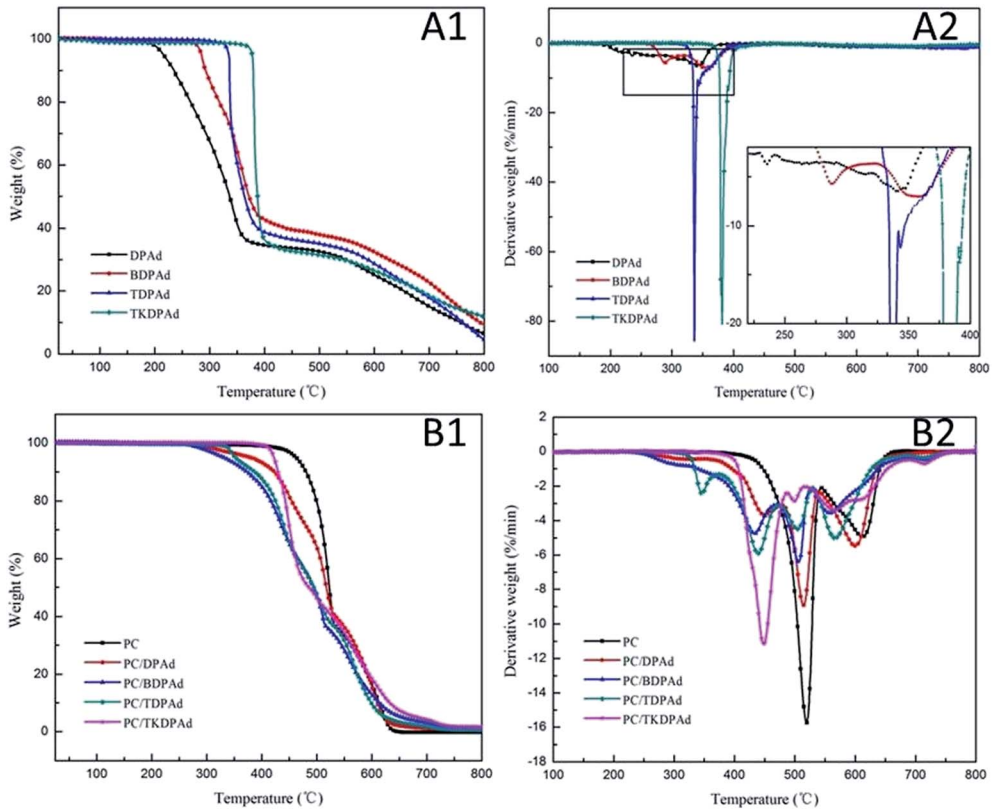

Fig. 5 TGA curves of FRs (A1 and A2) and PC and PC/FR (B1 and B2) under air atmosphere.

enhancement of the thermal stability upon more intercalation of phosphate. DPAd showed $T_{5\%}$ at 215.7 °C in air whereas BDPAd and TDPAd degraded between 284.8 °C and 334.9 °C. Notably, a two-stage dramatic weight loss of TKDPAd occurred at 377.5 °C. The results indicated that TKDPAd has the highest char yield of that of the other three FRs, even greater than the commercial RDP,[39] which means that the introducing of the bridging unit, adamantane, can improve the thermal stability of the FR. Moreover, the char yields increased as more phosphorus and substitution amounts are introduced except TDPAd.

The onset of degradation occurring at lower temperature with 8 wt% add-on FRs in contrast with the neat PC at below 422.5 °C were presented in Fig. 5B (Fig. 5B1 for TG curves and Fig. 5B2 for DTG curves). When 8 wt% of FRs was added to the PC, the initial thermal degradation occurs at a lower temperature. In contrast to literature report,[40] TGA experiments only showed scarcely any charring for the neat PC (0%) at 800 °C. The decomposition mechanism of PC under air was investigated by Jang *et al.*[15] and was found to mainly take place *via* chain scission of the isopropylidene linkage. However, the TG results presented in Fig. 5B1 clearly show that the amount of charred residue of composites containing FR is directly proportion to the char yielding behaviors of FRs discussed in previous section. For compositions of PC with DPAd and TDPAd, respectively, slightly increased amounts of residual char were found (0.9 and 0.5 wt%, respectively). In the case of the PC/BDPAd and PC/TKDPAd compositions, the amount of residual char after heating to 800 °C was relatively high (1.2 and

Table 3 TGA data of the FRs, PC and PC/FR in this study

Sample	$T_{5\%}$ (°C)	T_{max1} (°C)	T_{max2} (°C)	T_{max3} (°C)	T_{max4} (°C)	Residue at 800 °C (wt%)
DPAd	215.7	235.7	340.7			6.4
BDPAd	284.8	287.8	358.8			9.0
TDPAd	334.9	336.9	343.4			4.5
TKDPAd	377.5	381.5	391.5			11.8
PC	461.7			519.2	612.2	0.0
PC/DPAd	376.4		449.4	514.4	599.9	0.9
PC/BDPAd	331.5		433.5	506.0	558.0	1.2
PC/TDPAd	352.0	346.0	439.0	504.5	566.5	0.5
PC/TKDPAd	422.5		448.0	499.0	565.5	1.6

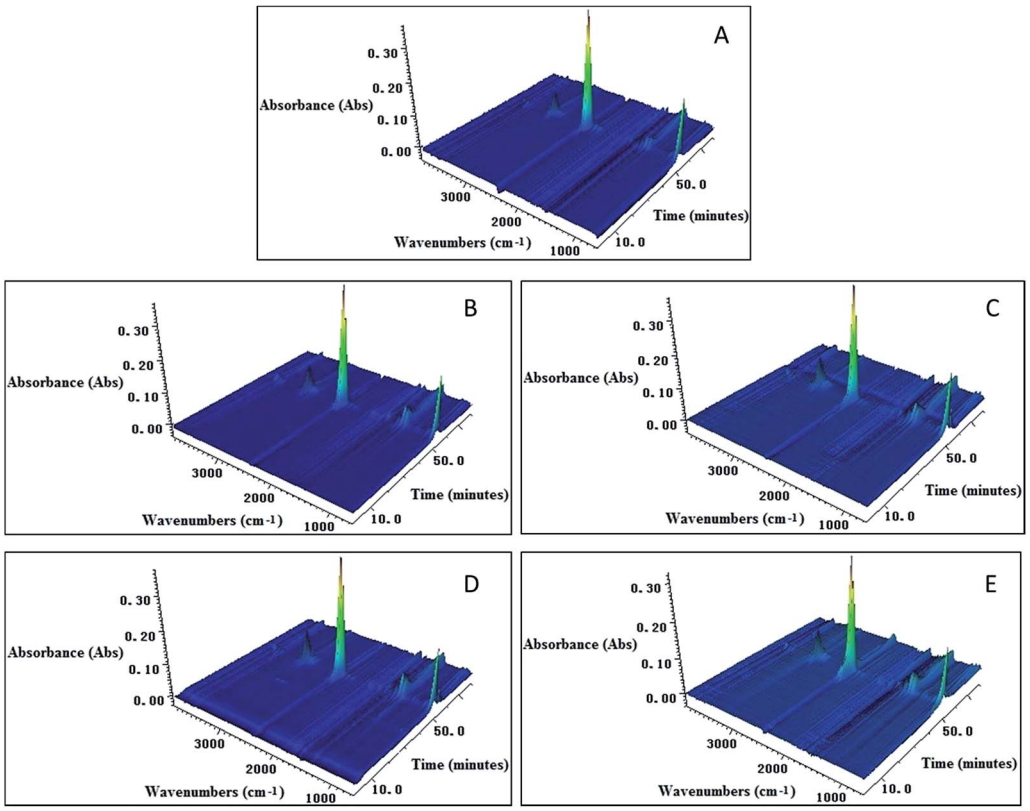

Fig. 6 Three-dimensional TGA-FTIR spectra of (A) PC, (B) PC/DPAd, (C) PC/BDPAd, (D) PC/TDPAd and (E) PC/TKDPAd.

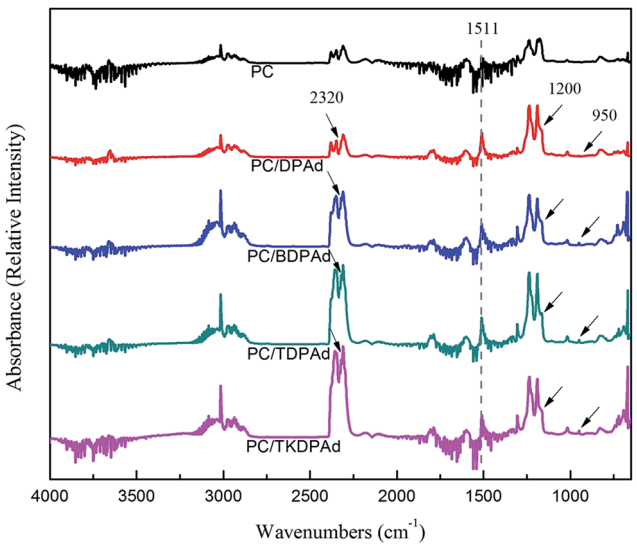

Fig. 7 FTIR spectra of pyrolysis products of PC, PC/DPAd, PC/BDPAd, PC/TDPAd and PC/TKDPAd at their maximum weight loss rates.

1.6 wt%, respectively). An interesting phenomenon can be seen that PC/TDPAd has four maximum decomposition temperatures, whereas PC/DPAd, PC/BDPAd and PC/TKDPAd have three of that. Furthermore, the amount of residual char of PC/TDPAd was found to be the least among the FRs in this study, which may be attributed to the resin state of TDPAd. Even though no discernible increase in the amount of charred residue is observed, the superior flame-retarding performance of TKDPAd is believed to be closely related to its char forming ability and high thermal stability. That is, the condensed phase mechanism is known to be the dominating action for the flame retardancy of PC.[18] Therefore, the flame retardancy of phosphorus-based FRs depends not only on the phosphorous content but also on the thermal stability of the phosphorus-based FRs.

3.3.2 TGA-FTIR analysis. The volatilized products from TGA furnace were inspected by a FTIR spectrometer simultaneously. Fig. 6 shows the three-dimensional (3D) TGA-FTIR spectra of gaseous phase in the thermal degradation of PC and PC/FR compositions, respectively. Fig. 7 shows the FTIR spectra of pyrolysis products of PC, PC/DPAd, PC/BDPAd, PC/TDPAd and PC/TKDPAd at their first maximum weight loss rates, respectively. The TGA-FTIR technique can give more information of volatilized products, which can help to better understand the thermal degradation mechanisms of PC/FR compositions.[41] Fig. 6 exhibits that the most obvious absorbance band in TGA-FTIR spectra of PC and PC/FR compositions is similar around 2379 cm^{-1}, which is the main product, carbon dioxide (CO_2). Furthermore, PC and PC/FR compositions exhibit nearly the same infrared absorbing time. In addition to the above information, no more can be directly detected from the 3D FTIR spectra. Fig. 7 shows that the other main volatilized products of the decomposition of PC and PC/FR compositions

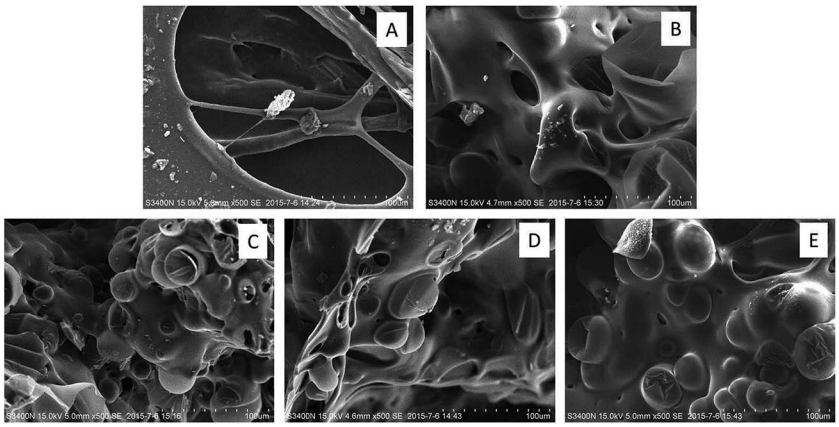

Fig. 8 SEM micrographs of the residual chars obtained from the LOI teat for (A) PC, (B) PC/DPAd, (C) PC/BDPAd, (D) PC/TDPAd and (E) PC/TKDPAd.

are released and also similar, such as water (H_2O, around 2379 cm^{-1}), carbon monoxide (CO, around 2180 cm^{-1}) and methane (CH_4, around 3016 cm^{-1}). Otherwise, some other important but not obvious peaks are listed: –OH (mainly include H_2O, phenol; around 3600 cm^{-1}), compounds containing aromatic ring (around 1600 cm^{-1}), and hydrocarbons (C–H stretching at around 1190 cm^{-1}).[42] Finally, the peak around 1787 cm^{-1} indicates the volatilized products containing carbonyl are released. These compounds are identified as carboxylic acid RCOOH (2977–2880 cm^{-1}, around 1787 cm^{-1}).[42] Moreover, the intensity of the carbonyl absorbance band (1787 cm^{-1}) to its nearby band (around 1600 cm^{-1}, aromatic rings vibration absorbance) in the spectra of PC/FR is higher with the increase of P content and substitution amounts of adamantane. It indicates that more carbon char structures are presented in PC/FR. Jang *et al.* also found that phosphate may stabilize carbon char from oxidative degradation in air atmosphere.[18] Besides, the weak peaks absorbance at 950 cm^{-1} and 1641 cm^{-1} which can be correspond to the phosphates (P–O) and P–OH stretching vibration, and the peak absorbance at 2320 cm^{-1} was assigned to P–H.[43,44] It is because the FRs reacted with PC mainly in the condensed phase as well as slightly in the gaseous phase during thermal degradation. And most phosphorous-containing components such as P–O–C, P–OH and P–H components were retained in the char residual rather than that in the gaseous phase during the thermal degradation. TGA results had been showed that the incorporation of adamantane-based phosphates into PC compositions promoted the formation of char residual, which trapped some of the volatile products and made them participate in the charring reaction. The char layer become a barrier and covered on the PC matrix which is effective to prohibit the heat flux and air incursion. This surface structure can improve the flame retardancy and thermal stability of PC compositions.

3.4 Analysis of residual char

3.4.1 Scanning electron microscopy (SEM). To further investigate how the FRs works in the PC/FR compositions, the morphology of the chars for the residues that left after LOI test are tested by SEM. As shown in Fig. 8A, there exists macroporous structure on the exterior surface of the neat PC. However, the interior char residue of the neat PC presents a

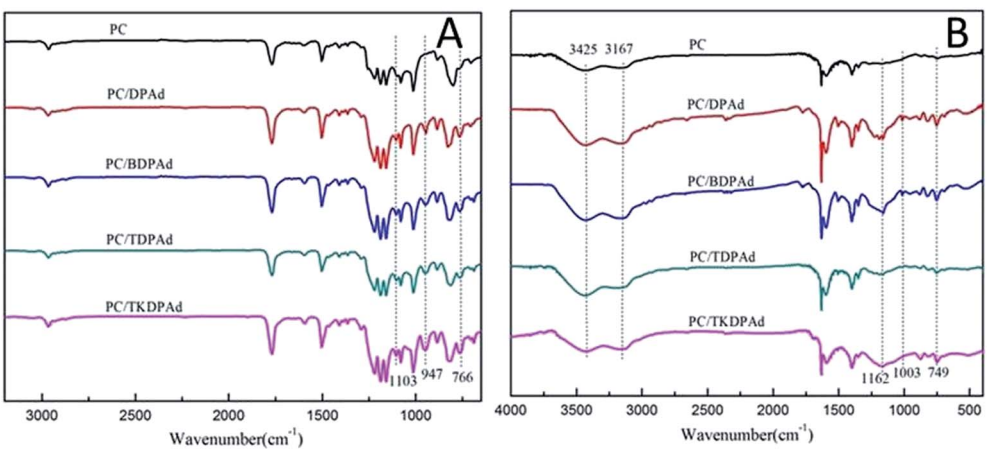

Fig. 9 FTIR curves of PC and PC/8 wt% FR before (A) and after (B) combustion under a synthetic air atmosphere.

smooth and continual char layer which means the rapid volatilization over the surface. This structure cannot provide a good barrier to stop the spread of the heat, oxygen and the emissions of volatile products. Compared to the sample of the neat PC, the surface of the sample of PC/FR compositions (Fig. 8B–E) mainly presents a continuous and protective carbon layer on which are dispersed bubbles and folds. And the compact order of the formed carbon layer is: PC/DPAd < PC/BDPAd < PC/TDPAd < PC/TKDPAd, which means that the quality of the formed carbon layer raises with the increase of the P content and the substitution amounts of adamantane. That also comes with the results of CCT. This means that the incorporation of the adamantane-based phosphates restricts the rapid volatilization at the surface and enhances the flame resistance of the char residue. From the analysis of CCT and SEM, the thermal degradation of the PC matrix proceeds fiercely under a high temperature in the process of combustion. So the combustion behaviors of FRs could be summarized: a fast degradation is preceded under high temperature, and then a char layer was formed on the surface of the PC matrix. The FRs quickly decomposed to form phosphorus compounds in the PC matrix and released more combustible small molecules such as CO_2 dissociated from the FRs, so that the time to ignite the PC compositions was decreased, which was shown in Fig. 4A. However, part of the FRs is pushed on the surface of the PC matrix by the volatile products such as H_2O, CO_2 and phenol derivates.[45] The addition of the FRs incorporated the adamantane as the bridging unit into PC enhanced thermal oxidative stability of the char layer formed on the surface of the PC matrix. Then the layer char prevented heat and oxygen into underlying polymeric substrate to block the series of thermo-oxidative reactions and the release of volatile products of underlying polymeric substrate. So the value of HRR of the PC/FR compositions decreases. The efficiency of the FRs on the combustion and enhancement of thermal stability of the char layer result in the significantly flame retardant efficiency of the PC/FR compositions.

3.4.2 FTIR analysis. To understand better the char formation of these phosphorus-containing compounds, the degradation of these FRs was carried out under air. After that, the charred residues of PC/FR were analyzed spectroscopically by employing FTIR. The FTIR spectra of before and after combustion of PC and PC/FR compositions were shown in Fig. 9. Fig. 9A exhibited the characteristic P–O–C (aromatic) group absorption at 1103 cm^{-1}. The 947 cm^{-1} is attributed to the absorptions of resonances of P═O and the 766 cm^{-1} stretch is caused by the attachment of phosphonate group on the adamantane ring. Fig. 5B show the FT-IR spectrum of after combustion of PC and PC/FR compositions. The intensities of the absorption bands at 3425 and 1003 cm^{-1} are attributed to the stretching of P–OH group, and the absorption peak at 1162 cm^{-1} is attributed to P═O and P–H.[45] A weak characteristic band at 2360 cm^{-1} is attributed to the P–H stretching vibration. Stretch at 3167 cm^{-1} is attributed to the absorptions of resonances of aromatic. The absorption band at 1003 cm^{-1} corresponds to P–O–C stretching. Moreover, the 749 cm^{-1} stretch of the PC/FR is caused by phosphonate group on the adamantane ring. It therefore becomes clear that the O–H structure is contained in the charred residue of the FRs.

Combine with the TGA and SEM results, the decomposition of the FRs proceeds with the cleavage of the P–O bond and consequent generation of phosphorus compounds, which promote the formation of a continuous and protective carbon layer. As shown previously, it can be inferred that the formation of the sharp degradation products from TKDPAd are the main reason for the observation of larger amount of charred residue from TKDPAd than the other FRs. It is speculated that the mainly sharp one degradation path of TKDPAd is responsible for the generation of phosphorus compounds, which leads to the formation of a continuous and protective carbon layer.[46]

4. Conclusions

In an attempt to investigate the factors affecting the flame-retarding behaviors of phosphorus-based FRs, a series of adamantane-based phosphorus derivatives were successfully synthesized and used to impart flame resistance to PC, their thermal degradation and flame-retarding performances were compared with each other. In TGA results, the FRs containing more diphenyl phosphoryl substituents were degraded at higher temperatures and produced a moderate amount of char yields at elevated temperature, which was related to the generation of phosphorus compounds that lead to the formation of the continuous and protective carbon layer in the charred residues. This tendency to generate a large amount of phosphorus compounds is beneficial to the condensed phase flame retardancy mechanism, and the TKDPAd shows the best flame retardancy (UL-94 V-0 ratings at 8 wt% loading) on PC compare to the other three FRs. And the analysis results of TGA and TGA-FTIR show that the flame retardancy mechanism of these adamantane-based phosphates are mainly in the condensed phase as well as slightly in the gaseous phase during the thermal degradation. It is concluded that the flame retardancy of phosphorus-based FRs depends not only on their phosphorous content but also on their thermal stability. And even though the phosphorous content of TKDPAd and RDP is nearly, but the introduction of adamantly increased TKDPAd's thermal stability compared with RDP in this study. The results revealed that TKDPAd was an efficient flame retardant for PC.

Acknowledgements

This work was supported by National Natural Science Foundation of China (Grant no. 21476051) and Science and Technology Project of Guangdong Province (Grant no. 2013B010403028).

Notes and references

1 S. Y. Lu and I. Hamerton, *Prog. Polym. Sci.*, 2002, **27**, 1661–1712.
2 C. Hoffendahl, G. Fontaine, S. Duquesne, F. Taschner, M. Mezgerb and S. Bourbigot, *RSC Adv.*, 2014, **4**, 20185–20199.

3 S. J. Chen, J. Li, Y. K. Zhu and S. P. Su, *RSC Adv.*, 2014, **4**, 32902–32913.
4 H. Li, J. Q. Zhao, S. M. Liu and Y. C. Yuan, *RSC Adv.*, 2014, **4**, 10395–10401.
5 S. V. Levchik and E. D. Weil, *J. Fire Sci.*, 2006, **24**, 137–151.
6 B. Swoboda, S. Buonomo, E. Leroy and J. M. Cuesta Lopez, *Polym. Degrad. Stab.*, 2008, **93**, 910–917.
7 A. Toldy, B. Szolnoki, I. Csontos and G. Marosi, *J. Appl. Polym. Sci.*, 2014, **131**, 40105–40112.
8 S. V. Levchik and E. D. Weil, *J. Fire Sci.*, 2006, **24**, 345–364.
9 M. Yin, L. Yang, X. Y. Li and H. B. Ma, *J. Appl. Polym. Sci.*, 2013, **130**, 2801–2808.
10 W. C. Zhang, X. M. Li, H. B. Fan and R. J. Yang, *Polym. Degrad. Stab.*, 2012, **97**, 2241–2248.
11 J. P. Ding, Z. Q. Tao, X. B. Zuo, L. Fan and S. Y. Yang, *Polym. Bull.*, 2009, **62**, 829–841.
12 Z. Wang, W. Wu, Y. H. Zhong, M. Z. Ruan and L. L. Hui, *J. Appl. Polym. Sci.*, 2015, **132**, 41545–41555.
13 K. A. Salmeia and S. Gaan, *Polym. Degrad. Stab.*, 2015, **113**, 119–134.
14 V. Benin, X. M. Cui, A. B. Morgan and K. Seiwert, *J. Appl. Polym. Sci.*, 2015, **132**, 42296–42305.
15 N. N. Tian, J. Gong, X. Wen, K. Yao and T. Tang, *RSC Adv.*, 2014, **4**, 17607–17614.
16 Z. J. Jiang, S. M. Liu, J. Q. Zhao and X. B. Chen, *Polym. Degrad. Stab.*, 2013, **98**, 2765–2773.
17 K. H. Pawlowski and B. Schartel, *Polym. Int.*, 2007, **56**, 1404–1414.
18 B. N. Jang and C. A. Wilkie, *Thermochim. Acta*, 2005, **433**, 1–12.
19 B. Perret, K. H. Pawlowski and B. Schartel, *J. Therm. Anal. Calorim.*, 2009, **97**, 949–958.
20 E. Wawrzyn, B. Schartel, M. Ciesielski, B. Kretzschmar, U. Braun and M. Döring, *Eur. Polym. J.*, 2012, **48**, 1561–1574.
21 M. C. Despinasse and B. Schartel, *Thermochim. Acta*, 2013, **563**, 51–61.
22 C. Nguyen and J. Kim, *Polym. Degrad. Stab.*, 2008, **93**, 1037–1043.
23 M. C. Despinasse and B. Schartel, *Polym. Degrad. Stab.*, 2012, **97**, 2571–2580.
24 D. Q. Hoang, J. Kim and B. N. Jang, *Polym. Degrad. Stab.*, 2008, **93**, 2042–2047.
25 K. A. Salmeia, J. Fage, S. Liang and S. Gaan, *Polymers*, 2015, **7**, 504–526.
26 H. Vothi, C. Nguyen and J. Kim, *Polym. Degrad. Stab.*, 2010, **95**, 1092–1098.
27 R. C. Fort and P. R. Schleyer, *Chem. Rev.*, 1964, **64**, 277–300.
28 Y. Hu and S. B. Sinnot, *Surf. Sci.*, 2003, **526**, 230–242.
29 L. Bauer and K. K. Khullar, *J. Org. Chem.*, 1971, **36**, 3038–3040.
30 W. Azzam, A. Bashir and O. Shekhah, *Appl. Surf. Sci.*, 2011, **257**, 3739–3747.
31 A. Z. Halimehjani, K. Marjani, A. Ashouri and V. Amani, *Inorg. Chim. Acta*, 2011, **373**, 282–285.
32 H. Zhu, J. W. Guo, C. F. Yang, S. Liu, Y. D. Cui and X. Zhong, *Synth. Commun.*, 2013, **43**, 1161–1167.
33 S. Liu, J. W. Guo and D. M. Jia, CN 1,974,515 A, issued June 06, 2007.
34 J. S. Wang, G. H. Wang, Y. Liu, Y. H. Jiao and D. Liu, *Ind. Eng. Chem. Res.*, 2014, **53**, 6978–6984.
35 J. W. Gilman, C. L. Jackson and A. B. Morgan, *Chem. Mater.*, 2000, **12**, 1866–1871.
36 J. Feng, J. W. Hao, J. X. Du and R. J. Yang, *Polym. Degrad. Stab.*, 2012, **97**, 605–614.
37 P. Y. Jia, M. Zhang, C. G. Liu, L. H. Hu, G. D. Feng, C. Y. Bo and Y. H. Zhou, *RSC Adv.*, 2015, **5**, 41169–41178.
38 Z. Hu, L. Chen, B. Zhao, Y. Luo, D. Y. Wang and Y. Z. Wang, *Polym. Degrad. Stab.*, 2011, **96**, 320–327.
39 B. N. Jang and C. A. Wilkie, *Thermochim. Acta*, 2005, **433**, 1–12.
40 B. N. Jang and C. A. Wilkie, *Thermochim. Acta*, 2005, **426**, 73–84.
41 T. Xu and X. M. Huang, *Fuel*, 2010, **89**, 2185–2190.
42 X. D. Qian, L. Song, Y. Hu, R. K. Yuen, L. J. Chen, Y. Q. Guo, N. N. Hong and S. H. Jiang, *Ind. Eng. Chem. Res.*, 2011, **50**, 1881–1892.
43 A. I. Balabanovich, *Thermochim. Acta*, 2005, **435**, 188–196.
44 L. Song, Q. L. He, Y. Hu, H. Chen and L. Liu, *Polym. Degrad. Stab.*, 2008, **93**, 627–639.
45 J. Wang, J. S. Yi and X. F. Cai, *J. Appl. Polym. Sci.*, 2011, **120**, 968–973.
46 V. Hai, H. Soekmin, N. Congtranh, B. Imhyuck and K. Jinhwan, *Fire Mater.*, 2014, **38**, 36–45.